Catalysis Today 182 (2012) 60–66

Contents lists available at ScienceDirect

Catalysis Today

journal homepage: www.elsevier.com/locate/cattod

Reduction processes in Cu/SiO_2, Co/SiO_2, and $CuCo/SiO_2$ catalysts

Miranda L. Smith, Andrew Campos, James J. Spivey*

Cain Department of Chemical Engineering, Louisiana State University, 110 Chemical Engineering, South Stadium Rd., Baton Rouge, LA 70803, USA

ARTICLE INFO

Article history:
Received 10 May 2011
Accepted 10 July 2011
Available online 16 September 2011

Keywords:
XANES
XRD
TPR
Copper
Cobalt
Reduction

ABSTRACT

Cu/SiO_2, Co/SiO_2, and bimetallic $CuCo/SiO_2$ catalysts have been synthesized and their reduction behavior characterized by TPR, *in situ* XRD, and *in situ* XANES. In Cu/SiO_2, a two step reduction process, $CuO \rightarrow Cu_2O \rightarrow Cu^0$, occurred. Two forms of the intermediate Cu_2O with different degrees of reducibility were observed. Addition of cobalt to Cu/SiO_2 resulted in formation of an amorphous fraction of CuO that was more easily reducible than crystalline CuO. Cobalt addition also prevented formation of the less reducible form of Cu_2O. Addition of copper to Co/SiO_2 increased the reducibility of Co_3O_4, and to greater extent of the intermediate CoO, which in the monometallic Co/SiO_2 was less readily reduced due to interaction with the support.

1. Introduction

Catalysts based on copper and cobalt have been studied for hydrogenation of CO to mixtures of ethanol and higher alcohols. This reaction is thought to occur by a dual site mechanism: CO associatively adsorbed on one type of site is inserted into surface hydrocarbon species arising from CO dissociation on the other site [1,2]. Hydrogenation of the resulting intermediate yields the alcohol. The site pairs mainly responsible for alcohol synthesis are often proposed to be Cu^0 and Co^0 in close interaction or proximity [1,3,4], but have occasionally been identified as $Co^0/Co^{\delta+}$ pairs, with copper maintaining this state of reduction [5]. In fact, the nature of the active centers may depend on the activation conditions applied to the catalyst [6]. Therefore, it is important to understand reduction processes in both copper–cobalt catalysts and their monometallic counterparts.

Bulk unsupported CuO normally reduces in a single step to Cu^0, without formation of a Cu_2O intermediate [7,8]. Copper oxide becomes reducible at lower temperature when supported on silica than when unsupported, due to increased dispersion and greater reactivity toward H_2 [9–11]. Sometimes multiple peaks are observed during temperature programmed reduction (TPR) of Cu/SiO_2 catalysts. In such cases, some authors associate the lower temperature peak with reduction of a CuO phase of low crystallinity and small particle size, presumably forming Cu^0 directly [11–14]. Others claim small CuO particles should interact with SiO_2, hindering reduction [10]. Moreover, if the area ratio of these TPR peaks is ~1:1, then the possibility of a sequential reduction, $CuO \rightarrow Cu_2O \rightarrow Cu$, must also be considered.

Co/SiO_2 catalysts typically reduce in two steps: $Co_3O_4 \rightarrow CoO \rightarrow Co^0$ [15–17]. The second step, in particular, is impeded by support interactions that become important when the particle size is small [15]. Divalent cobalt species show increasing difficulty of reduction in the following order: Co^{2+} with little support interaction, Co^{2+} having slightly stronger interaction with SiO_2, cobalt hydrosilicates, and cobalt silicate [16]. Cobalt silicate, which is favored by high-pH preparation conditions, shows a TPR maximum at about 900 °C [16].

TPR of unsupported, coprecipitated, air-calcined oxides of cobalt and copper shows that the presence of copper promotes the reduction of Co_3O_4 [18]. $CuCo/SiO_2$ catalysts usually show a single TPR peak at lower temperature than is typical for reduction of cobalt oxides [19–21]. Different authors have assumed a strong interaction between CuO and Co_3O_4 [18,19,21] or even formation of a $Cu_xCo_{3-x}O_4$ phase [18,20] to explain the promoting effect of copper on cobalt reduction.

Catalyst reduction pathways depend on preparation method, thermal treatment, and metal loading and can be quite complex even in monometallic systems. Addition of a second metal complicates the system even further. Therefore, a thorough characterization of the activation process is a prerequisite for understanding the nature of active species in each catalyst. The objective of this work is to apply complementary characterization techniques (TPR, *in situ* XRD, and *in situ* XANES) to study the effects of copper and cobalt upon each other during reduction of SiO_2-supported catalysts.

* Corresponding author. Tel.: +1 225 578 3690; fax: +1 225 578 1476.
E-mail address: jjspivey@lsu.edu (J.J. Spivey).

0920-5861/$ – see front matter © 2011 Elsevier B.V. All rights reserved.
doi:10.1016/j.cattod.2011.07.026

2. Materials and methods

2.1. Catalyst preparation

Three catalysts were prepared by incipient wetness impregnation of SiO_2 (PQ Corporation) with an aqueous solution of $Cu(NO_3)_2{\cdot}2.5H_2O$ alone, $Co(NO_3)_2{\cdot}6H_2O$ alone, or both these salts together. The catalysts were dried overnight (17 h) at 100–105 °C. They were calcined in a tube furnace in stagnant air by ramping at 4 °C/min to 500 °C and maintaining that temperature for 2 h.

The designations and nominal compositions, on a post-reduction basis, of the three catalysts are as follows: (1) Cu/SiO_2, 3.5 wt% Cu; (2) Co/SiO_2, 3.5 wt% Co; and (3) $CuCo/SiO_2$, 3.5 wt% Cu, 3.5 wt% Co.

2.2. Composition and texture

The actual compositions of the calcined catalysts were determined by ICP-OES using a Perkin Elmer 2000 DV ICP-optical emission spectrometer.

Flow BET measurements were performed in an Altamira AMI-200 system. About 40 mg of calcined catalyst was pretreated in 30 sccm He at 150 °C for 30 min. N_2 concentrations of 10%, 20%, and 30% in a He carrier were used for the adsorption. BET surface area was calculated based on N_2 adsorption at liquid nitrogen temperature.

2.3. Temperature programmed reduction (TPR)

TPR experiments were carried out in an Altamira AMI-200 system. The catalyst (45 mg) was dried in 30 sccm He at 120 °C for 100 min. After cooling to room temperature, the catalyst was exposed to 30 sccm of 10% H_2/Ar flow as the temperature ramped at 10 °C/min to 750 °C. H_2 consumption was monitored by a thermal conductivity detector (TCD). Calibration of the TCD by TPR of Ag_2O enabled quantitative evaluation of H_2 consumption.

2.4. In situ X-ray diffraction (XRD)

XRD experiments were done at the Center for Nanophase Materials Sciences, Oak Ridge National Laboratory, Oak Ridge, TN. The catalyst sample was loaded into an Anton Paar XRK900 reaction chamber and exposed to 4% H_2/He flow. XRD patterns were recorded at selected temperatures by a PANalytical X'Pert Pro MPD diffractometer using Cu Kα radiation. The scan speed was 0.030384°/s, and the step size was 0.017°.

Phase identification was carried out by the Search & Match feature of X'Pert HighScore Plus (v. 3.0) using the library provided by the Crystallography Open Database.

2.5. In situ X-ray absorption near edge structure (XANES)

XANES measurements were collected on the Double Crystal Monochromator (DCM) beamline at the J. Bennett Johnston, Sr., Center for Advanced Microstructures and Devices (CAMD), Baton Rouge, LA. About 20 mg of sample was mixed with 20 mg of amorphous SiO_2 and loaded into a Lytle cell. As a 10% H_2/Ar mixture flowed over the catalyst, the temperature was increased at 2 °C/min to 362 °C.

XANES spectra were collected at the Cu K-edge of $CuCo/SiO_2$ and the Co K-edge of Co/SiO_2 and $CuCo/SiO_2$. During the temperature ramp, scans were collected using the following parameters: 1 eV steps in the range −50 to −15 eV relative to the edge, 0.5 eV steps in the range −15 to 50 eV, and 1 eV steps in the range 50–100 eV. The integration time at each data point was 1 s. A foil reference of the element being measured was placed in the beam path beyond the sample and scanned in transmission mode.

Transmission data were processed and analyzed in the Athena (v. 0.8.061) component of the Ifeffit software [22]. First, the edge energy of the foil reference (taken as the maximum in the first derivative of its spectrum) was shifted to its literature value (8979 eV for Cu, 7709 eV for Co) [23]. Each simultaneously measured sample spectrum was calibrated according to that shift. The spectra were processed by deglitching and determination of the pre-edge line and normalization range. Next, each spectrum was analyzed by linear combination fitting (LCF) of its derivative to the derivative spectra of reference standards. The Cu standards included CuO, Cu_2O, and Cu^0 foil. The Co standards included Co_3O_4, CoO, and Co^0 foil. The model adopted for each fitting each spectrum was selected by a combinatorial approach, using all three standards and all possible combinations of two standards. Of the four possible fits, the one with the lowest χ^2_ν value was chosen. Each fit was confined to the region of the derivative spectrum that showed clear peaks.

Table 1
Catalyst surface areas, determined by flow BET, and compositions, determined by ICP-OES.

Catalyst	S_{BET} (m^2/g)	Composition (wt%)	
		Co	Cu
Cu/SiO_2	261 ± 14	–	3.30 ± 0.06
Co/SiO_2	268 ± 11	2.99 ± 0.15	–
$CuCo/SiO_2$	251 ± 4	2.97 ± 0.02	3.18 ± 0.09

3. Results

3.1. Composition and texture

BET and ICP-OES results are listed in Table 1. The surface areas of all the catalysts, according to N_2 adsorption, are between 250 and 270 m^2/g. The surface area of calcined SiO_2 is 279 m^2/g.

3.2. TPR

TPR profiles of the three catalysts are shown in Fig. 1. Cu/SiO_2 exhibits a main peak at 220 °C, with a high temperature shoulder and another small feature at 300 °C. The Co/SiO_2 profile contains a broad area of hydrogen consumption, spanning from 220 °C to 600 °C and apparently consisting of several overlapping reduction

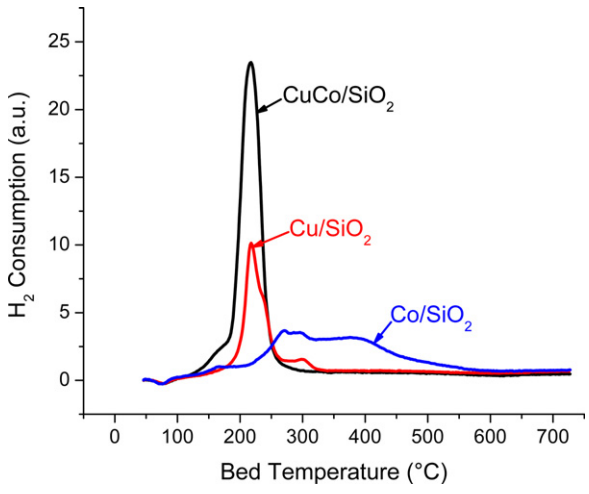

Fig. 1. TPR profiles in 10% H_2/Ar, ramping at 10 °C/min.

Table 2
Quantitative H_2 consumption during TPR.

Catalyst	H_2 consumption (mmol/g)	Expected H_2 consumption[a] (mmol/g)
Cu/SiO_2	0.65 ± 0.10	0.52
Co/SiO_2	0.76 ± 0.09	0.68
$CuCo/SiO_2$	1.50 ± 0.23	1.17

[a] Assuming complete conversion of CuO and Co_3O_4 to Cu^0 and Co^0, respectively.

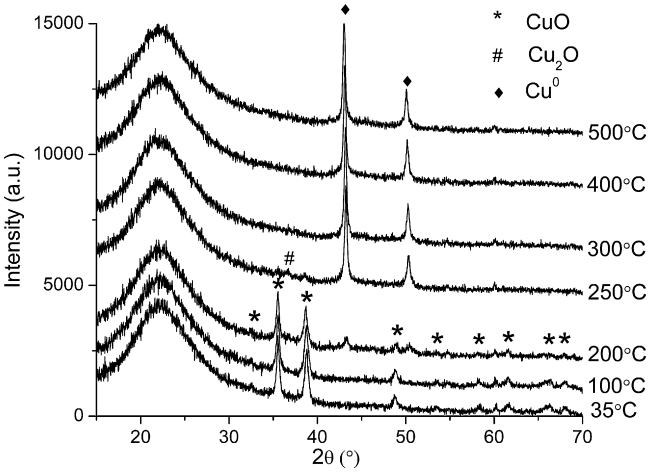

Fig. 2. XRD patterns of Cu/SiO_2 during reduction in 4% H_2/He at the indicated temperatures.

bands. Like that of Cu/SiO_2, the $CuCo/SiO_2$ TPR shows a prominent peak at 220 °C, but its shoulder is on the low temperature side.

Quantities of hydrogen consumed by each catalyst are listed in Table 2. In each case, the catalyst consumes sufficient hydrogen to reduce CuO, when present, to Cu^0 and Co_3O_4, when present, to Co^0. In addition, the hydrogen consumption by $CuCo/SiO_2$ is near the sum of the total uptakes by Cu/SiO_2 and Co/SiO_2.

3.3. *In situ* XRD

The XRD patterns of Cu/SiO_2 during isothermal hydrogen reduction at selected temperatures are shown in Fig. 2. This catalyst initially contains CuO, as expected. With increasing temperature, the crystalline phases in Cu/SiO_2 transform as follows. At 200 °C, a small amount of Cu^0 appears. At 250 °C, CuO almost disappears, and Cu^0 is the dominant phase. A minor peak at $2\theta = 36.6°$ and $d = 2.45$ suggests also the presence of a small amount of Cu_2O [14,24,25]. By 300 °C, Cu^0 is the only remaining phase detected by XRD.

The XRD patterns of Co/SiO_2 during reduction (Fig. 3) show that Co_3O_4 is the starting crystalline phase, which transforms to CoO by 300 °C. At 400 °C, CoO has begun converting to a cubic Co^0 phase, but this process is complete only after an extended time at 600 °C.

$CuCo/SiO_2$ initially contains crystalline CuO and Co_3O_4 (Fig. 4). At 200 °C, metallic phases have begun to appear. Intermediates such as Cu_2O and CoO may also be present at this stage, though interference from other peaks hinders this determination. By 300 °C, only metallic crystalline phases remain.

The sizes of crystallites in the three catalysts were determined by the Scherrer method with correction for instrumental broadening. Table 3 shows the changing crystallite sizes with increasing temperature.

CuO crystallites are slightly larger in Cu/SiO_2 (21–26 nm) than in $CuCo/SiO_2$ (19–20 nm). In addition, at room temperature, the area of the CuO (1 1 1) peak (not shown) is 50% less in $CuCo/SiO_2$ than in Cu/SiO_2. The copper metal loading (from ICP) is only about 4% lower in $CuCo/SiO_2$ than in Cu/SiO_2. Thus, the bimetallic catalyst contains both crystalline and noncrystalline CuO.

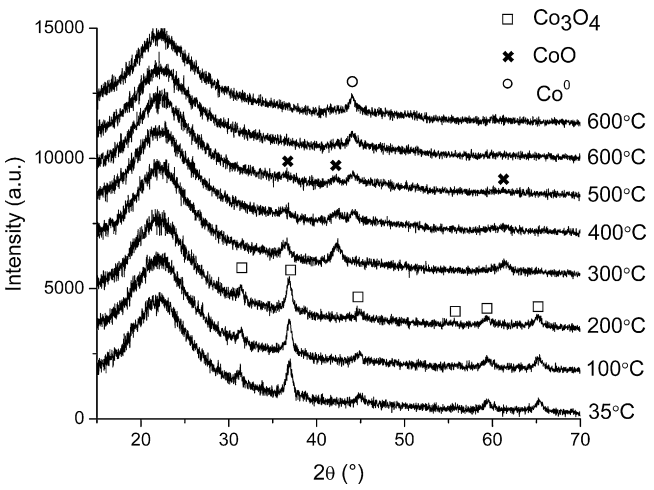

Fig. 3. XRD patterns of Co/SiO_2 during reduction in 4% H_2/He at the indicated temperatures. A second scan was collected at 600 °C immediately after the first.

When Cu^0 appears in Cu/SiO_2, crystallites initially have an average diameter of 22.4 nm (200 °C), but enlarge to 57.1 nm at 250 °C and 62–66 nm at higher temperatures. These sizes, from Table 3, were calculated based on the Cu^0 (1 1 1) peak. If instead the Scherrer formula is applied to the Cu^0 (2 0 0) peak, the Cu^0 crystallite diameter is 11.6 nm at 200 °C, 32.6 nm at 250 °C, and 44–47 nm at 300–500 °C. If the (1 1 1) plane is assumed parallel to the support, the different dimensions obtained from different peaks suggest a flattened particle shape [26].

Co_3O_4 crystallite sizes fall into the same range (11–16 nm) in Co/SiO_2 and $CuCo/SiO_2$. However, at room temperature, the area of the Co_3O_4 (3 1 1) peak is 30% higher in $CuCo/SiO_2$ than in Co/SiO_2, whereas the cobalt metal loading is about the same in both catalysts. This suggests that more crystalline, and less amorphous, Co_3O_4 exists in $CuCo/SiO_2$ than in Co/SiO_2 at room temperature.

In Co/SiO_2, the intermediate CoO phase has a crystallite size of 7–12 nm. When Co^0 crystallites appear at 400–600 °C, they are similar in size. The final Co^0 crystallite size is close to 75% of the starting Co_3O_4 crystallite size, which would be expected on the basis of the molar volumes of Co^0 and Co_3O_4 [17,27]. Co^0 crystallites on Co/SiO_2 do not exhibit the marked sintering that Cu^0 crystallites do on Cu/SiO_2.

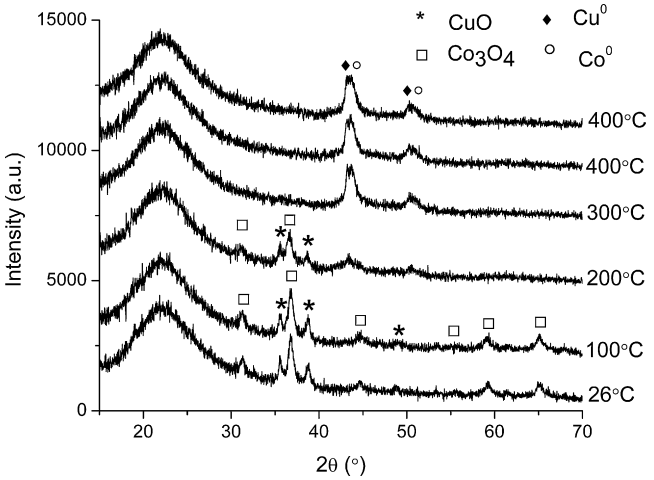

Fig. 4. XRD patterns of $CuCo/SiO_2$ during reduction in 4% H_2/He at the indicated temperatures. A second scan was collected at 400 °C immediately after the first.

Table 3
Crystallite size (nm), determined by the Scherrer method with correction for instrumental broadening.

Temperature (°C)	Cu/SiO_2		Co/SiO_2			$CuCo/SiO_2$	
	CuO[a]	Cu^0[a]	Co_3O_4[a]	CoO[a]	Co^0[a]	CuO[a]	Co_3O_4[a]
35 (26)[b]	24.8	–	12.7	–	–	19.6	15.2
100	21.6	–	15.0	–	–	20.0	13.7
200	25.5	22.4	13.7	–	–	19.0	11.0
250	–	57.1	–	–	–	–	–
300	–	62.1	–	8.6	–	–	–
400	–	65.7	–	7.5	10.0	–	–
500	–	65.6	–	11.5	7.6	–	–
600	–	–	–	–	8.8, 10.3[c]	–	–

[a] The crystallite size calculations are based on the following peaks: CuO (1 1 1), Cu^0 (1 1 1), Co_3O_4 (3 1 1), CoO (2 0 0), and Co^0 (1 1 1).
[b] Room temperature measurements were collected at 35 °C on Cu/SiO_2 and Co/SiO_2 and at 26 °C on $CuCo/SiO_2$.
[c] From back-to-back measurements at 600 °C.

The overlapping of the diffraction peaks of Cu^0 and Co^0 in $CuCo/SiO_2$ prevents accurate determination of their crystallite size. Overlapping or intermediate peaks can arise from intermediate lattice spacing between the spacings of pure Cu^0 and Co^0, due to alloying of the metals [28,29]. To address the question of possible alloying in $CuCo/SiO_2$, the diffraction patterns of Cu/SiO_2, Co/SiO_2, and $CuCo/SiO_2$ at 400 °C are compared in Fig. 5. The formation of CuCo alloy cannot be ruled out from this figure, although in general Cu^0 has limited solubility in Co^0 [6] and would be expected to segregate to the surface of such an alloy to lower the surface free energy [27].

3.4. *In situ* XANES

The XANES spectra and LCF results at the Co K-edge of Co/SiO_2, the Co K-edge of $CuCo/SiO_2$, and the Cu K-edge of $CuCo/SiO_2$ during temperature programmed reduction are shown in Figs. 6–8, respectively. The XANES spectra of cobalt and copper reference compounds are shown in Fig. 9. Sample LCFs from each *in situ* experiment are shown in Fig. 10.

Initially, Co_3O_4 is the only cobalt phase present in Co/SiO_2 (Fig. 6). At about 280 °C, the white line region of the spectrum begins to assume the more rounded shape of the CoO standard, which is confirmed by the appearance of CoO in the LCF profile. However, as Co_3O_4 reduces, the fit becomes imperfect in the white line region as shown in Fig. 10. Probably, Co_3O_4 reduces via CoO species that have varying degrees of interaction with the support. Electron deficiencies due to such interactions can result in enhanced white line intensities that cannot be perfectly modeled by reference spectra of bulk compounds [30]. Consequently, the full extent of Co_3O_4 conversion may not be completely captured by the LCF results in Fig. 6. Nevertheless, the spectra clearly show that appreciable Co_3O_4 reduction occurs by 280 °C. Furthermore, a small shoulder begins to develop at the absorption edge at 358 °C, denoting the first appearance of Co^0.

Fig. 7 shows the Co K-edge spectra and LCF results on $CuCo/SiO_2$. The low-temperature scans confirm that Co_3O_4 is the starting

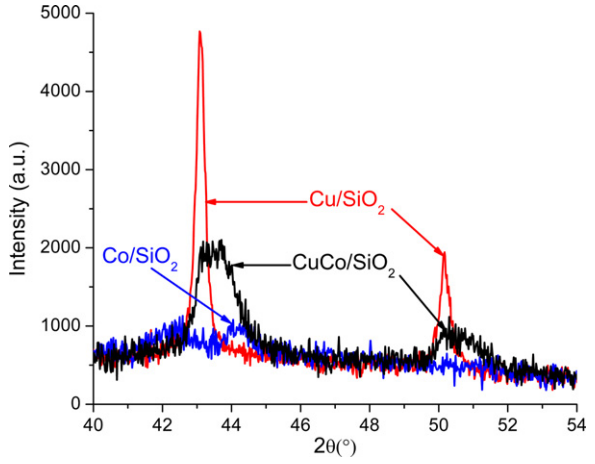

Fig. 5. XRD patterns of Cu/SiO_2, Co/SiO_2, and $CuCo/SiO_2$ during reduction in 4% H_2/He at 400 °C.

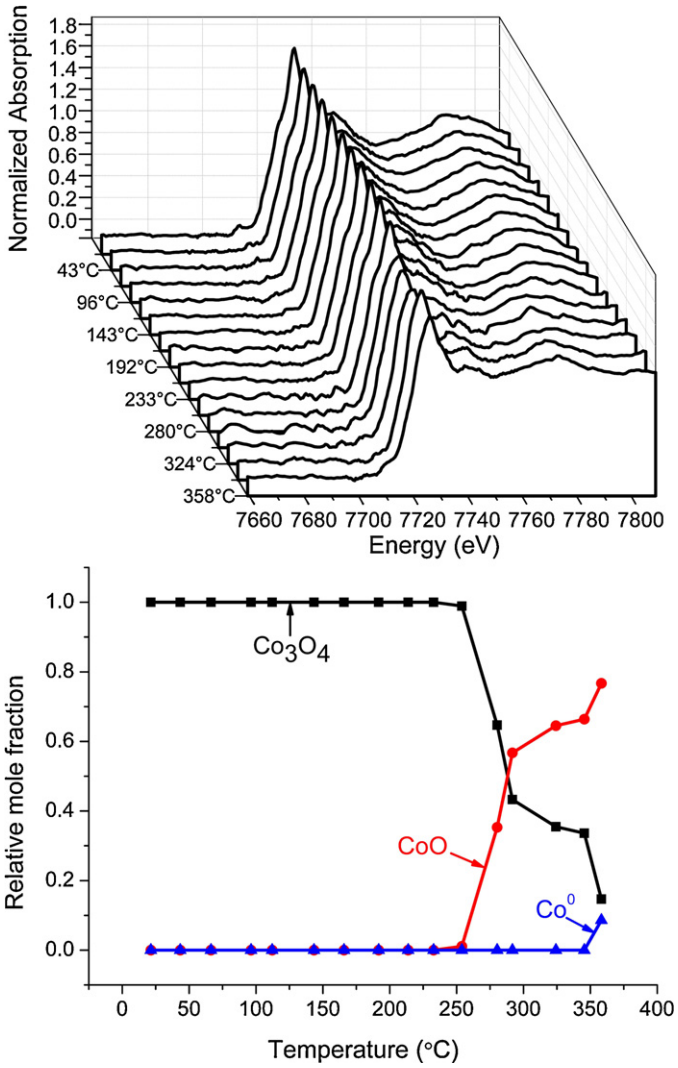

Fig. 6. Top: XANES spectra at the Co K-edge of Co/SiO_2 during temperature ramping at 2 °C/min in 10% H_2/Ar. Bottom: Composition of cobalt phases in Co/SiO_2, from LCF, as a function of temperature. Non-cobalt phases are excluded from the mole fractions.

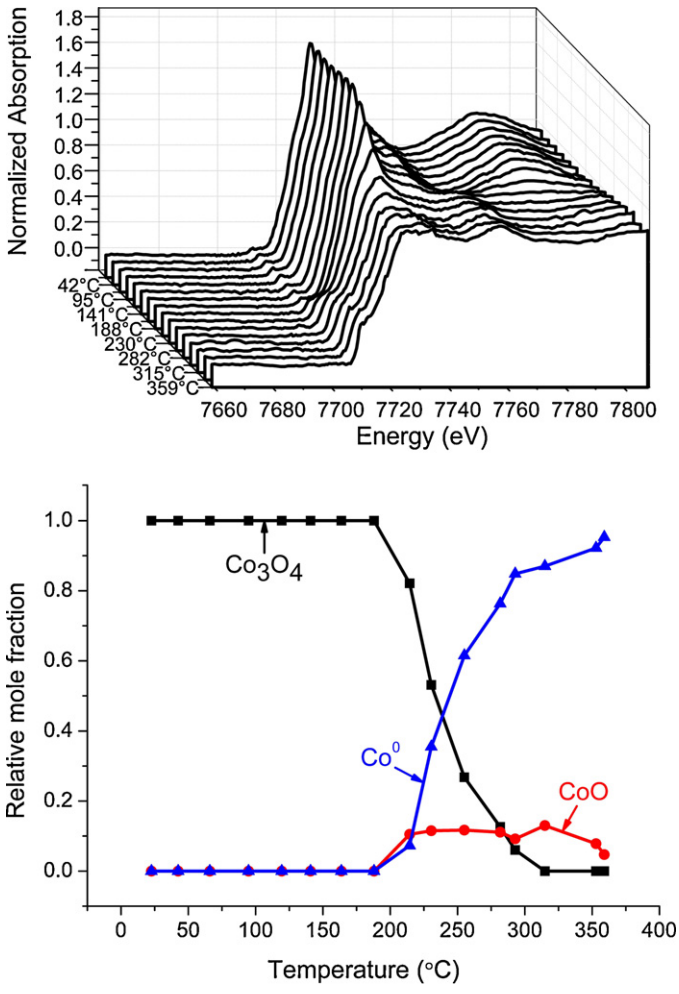

Fig. 7. Top: XANES spectra at the Co K-edge of $CuCo/SiO_2$ during temperature ramping at 2 °C/min in 10% H_2/Ar. Bottom: Composition of cobalt phases in $CuCo/SiO_2$, from LCF, as a function of temperature. Non-cobalt phases are excluded from the mole fractions.

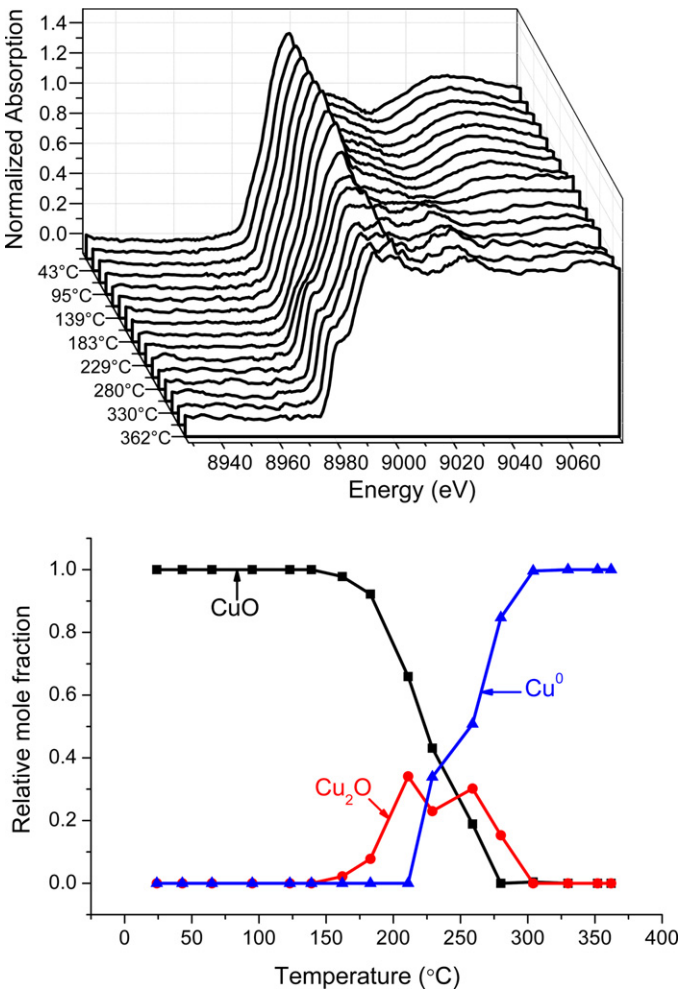

Fig. 8. Top: XANES spectra at the Cu K-edge of $CuCo/SiO_2$ during temperature ramping at 2 °C/min in 10% H_2/Ar. Bottom: Composition of copper phases in $CuCo/SiO_2$, from LCF, as a function of temperature. Non-copper phases are excluded from the mole fractions.

cobalt phase in this catalyst. Conversion to CoO begins at about 215 °C, 65 °C lower than for the monometallic Co/SiO_2 catalyst. This is also accompanied by a decrease in the white line intensity and growth of a shoulder at the edge, corresponding to the simultaneous appearance of Co^0 at the same temperature.

Fig. 8 shows the Cu K-edge spectra and LCF results on $CuCo/SiO_2$. When compared to the Cu reference standards in Fig. 9, the spectra up to 140 °C match that of CuO. In the early stages of reduction, CuO is converted first to Cu_2O. At about 230 °C, Cu^0 appears as well. By 300 °C, conversion to Cu^0 is complete.

4. Discussion

After isothermal reduction at 400 °C, Cu/SiO_2 would be expected to contain Cu^0, Co/SiO_2 to contain Co^0 and CoO, and $CuCo/SiO_2$ to contain a mixture of Cu^0 and Co^0. Thus, the reduction temperature can be manipulated in order to produce catalysts containing the desired species, whether Co^0/Cu^0 or Co^0/Co^{2+}.

4.1. Effect of Co addition to Cu/SiO_2

The low temperature shoulder in the TPR (Fig. 1) of $CuCo/SiO_2$ can be identified with the help of XRD and XANES results. From peak fitting of the TPR profile, the shoulder arises from a band at about 170 °C that accounts for 12.5% of the total hydrogen consumption by this catalyst. In the room temperature XRD patterns, comparison of the areas of the CuO (1 1 1) peak of Cu/SiO_2 and of $CuCo/SiO_2$ shows that this phase is more crystalline in Cu/SiO_2. Assuming that CuO in Cu/SiO_2 is fully crystalline, an estimated 50% of the CuO in $CuCo/SiO_2$ is noncrystalline. Thus, the main TPR peak at 220 °C (observed for both catalysts) involves reduction of crystalline CuO, and the shoulder at 170 °C (visible only in $CuCo/SiO_2$) corresponds to reduction of noncrystalline CuO. From XANES (Fig. 8), it is clear that CuO in $CuCo/SiO_2$ begins reducing to Cu_2O before 200 °C, before the appearance of metallic Cu, and before any reduction of Co_3O_4. Accordingly, the earlier conclusion can be extended to say the shoulder at 170 °C relates to reduction of noncrystalline CuO to Cu_2O. This point can be further corroborated by calculating the percentage of total H_2 consumption needed to reduce noncrystalline CuO (that is, 50% of total CuO in $CuCo/SiO_2$) to Cu_2O. This value comes to 10.7%, compared to 12.5% obtained by peak fitting. The slight discrepancy between the two values might have been introduced during profile fitting of the TPR and XRD patterns.

An alternative explanation for the decrease in crystalline CuO and increase in crystalline Co_3O_4 observed by XRD in $CuCo/SiO_2$ relative to the monometallic catalysts could be formation of a mixed oxide. A spinel-type oxide, with incorporated Cu, would be difficult to distinguish from Co_3O_4 by XRD [31,32]. However, the $Cu_xCo_{3-x}O_4$ phase shows low thermal stability, especially at

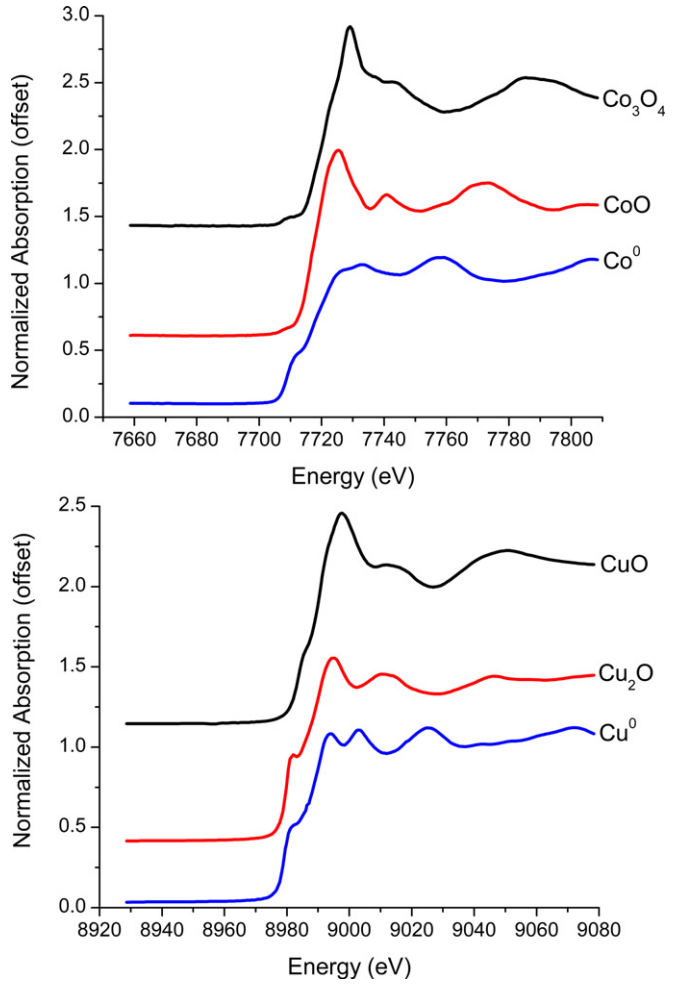

Fig. 9. Top: Co K-edge XANES spectra of reference standards (Co_3O_4, CoO, and Co^0) used in LCF of cobalt phases. Bottom: Cu K-edge XANES spectra of reference standards (CuO, Cu_2O, and Cu^0) used in LCF of copper phases.

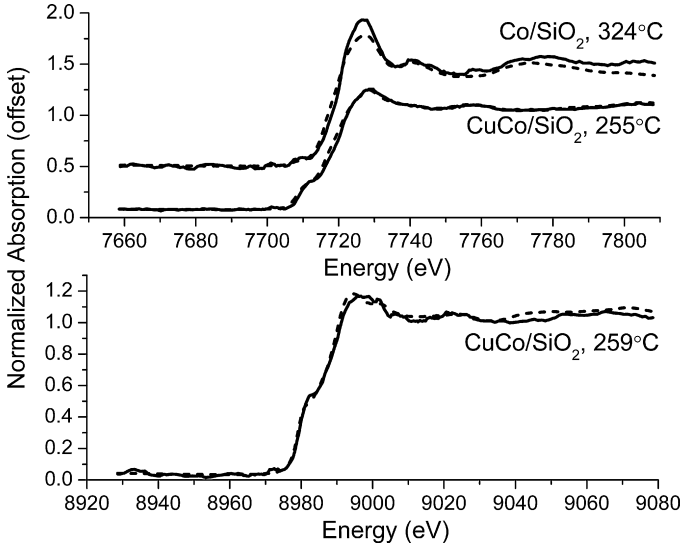

Fig. 10. Sample LCFs of Co K-edge spectra (top), including Co/SiO_2 at 324 °C and $CuCo/SiO_2$ at 255 °C, and a Cu K-edge spectrum (bottom) of $CuCo/SiO_2$ at 259 °C.

Cu/Co ratios as high as the one used in this work, and would be expected to decompose during the calcination at 500 °C [31]. Furthermore, XANES analysis does not support the formation of a copper–cobalt mixed metal oxide in the catalyst as-prepared or during reduction. For example, the XANES lineshapes from Cu^{2+} in CuO and in the octahedral sites of a spinel would be expected to differ markedly, by analogy to results obtained on CuO and $CuFe_2O_4$ (Fig. 3 of [33]). These reasons support the idea that the decrease in CuO diffraction peaks is due to creation of an amorphous fraction of CuO, not incorporation of Cu into the spinel phase.

The Cu/SiO_2 TPR profile (Fig. 1) has shoulders on the high, rather than low, temperature side. Peak fitting reveals that the main peak at 220 °C, already assigned to reduction of crystalline CuO, has an area approximately equal to the sum of the areas of the high temperature shoulder (240 °C) and small peak at 300 °C. From the stoichiometry of H_2 consumption for a stepwise reduction, this suggests that the main peak corresponds to reduction of CuO to Cu_2O, and the secondary peaks represent reduction of Cu_2O to Cu^0. From XRD (Fig. 2), residual crystalline Cu_2O is observed at 250 °C and converts to Cu metal during isothermal treatment at 300 °C. This confirms that Cu_2O is an intermediate during reduction of Cu/SiO_2.

The separation of Cu_2O reduction into two TPR peaks suggests that a fraction of the intermediate Cu_2O (about 26% of it) is especially difficult to reduce to Cu metal. It is not obvious why this should be so, but the type of Cu_2O that reduces with relative difficulty at 300 °C is not observed in $CuCo/SiO_2$.

4.2. Effect of Cu addition to Co/SiO_2

The reduction of Co/SiO_2 occurs over a wide temperature range, which implies the existence of many reducible species in varying degrees of interaction with the support [16]. The amplified white line of the Co K-edge spectra of reducing Co/SiO_2 suggests that the Co^{2+} species, in particular, are more electron deficient than in bulk CoO. In fact, the XANES spectra of CoO and Co_2SiO_4 are quite similar [17], the main difference being a more intense white line in the spectrum of the latter. Nevertheless, the formation of Co_2SiO_4, which reduces at temperatures greater than 800 °C [16,17], does not seem to occur on Co/SiO_2, which is completely reduced at 600 °C. According to the XRD results (Fig. 3), CoO itself is difficult to reduce on Co/SiO_2 and is observed across a wide temperature span, 300–500 °C. The strength of interaction of Co^{2+} with SiO_2 seems to lie somewhere between bulk unsupported CoO and Co_2SiO_4.

Co_3O_4 in $CuCo/SiO_2$ reduces simultaneously with crystalline CuO, at a temperature about 65 °C lower than the corresponding transformation in Co/SiO_2. The reduction of Co^{2+} is very efficiently promoted by copper. According to TPR and XRD, this process is complete by 300 °C on $CuCo/SiO_2$, whereas it continues up to 600 °C on Co/SiO_2. XANES also shows that the CoO intermediate is reduced almost as fast as it can be produced on $CuCo/SiO_2$, in marked contrast to the situation on Co/SiO_2. This indicates that an interaction between copper and cobalt phases exists, and it has a stronger effect on Co^{2+} reducibility than the cobalt-silica interaction, which would tend to maintain cobalt in an oxidized state.

5. Conclusions

CuO and Co_3O_4 reduce via two step processes- $CuO \rightarrow Cu_2O \rightarrow Cu^0$ and $Co_3O_4 \rightarrow CoO \rightarrow Co^0$, respectively, on SiO_2-supported monometallic and bimetallic catalysts. The effects of cobalt addition to a Cu/SiO_2 catalyst are (1) an increase in the dispersion and amorphous content of CuO, (2) creation of a more easily reducible (to Cu_2O) fraction of CuO, due to its higher dispersion, and (3) elimination of a type of Cu_2O that is relatively

difficult to reduce. The main effect of copper addition to a Co/SiO_2 catalyst is to increase the reducibility of cobalt oxides, especially of CoO.

Acknowledgments

This material is based upon work supported as part of the Center for Atomic Level Catalyst Design, an Energy Frontier Research Center funded by the U.S. Department of Energy, Office of Science, Office of Basic Energy Sciences under Award Number DE-SC0001058. A portion of this research was conducted at the Center for Nanophase Materials Sciences, which is sponsored at Oak Ridge National Laboratory by the Scientific User Facilities Division, U.S. Department of Energy. The help of Dr. Andrew Payzant and Dr. Viviane Schwartz in setting up the XRD experiments at ORNL is gratefully acknowledged. The assistance of Gregory Merchan, CAMD beamline scientist, with XANES experiments is also appreciated. ICP-OES analysis was carried out by Kimberly Hutchison (North Carolina State University, Department of Soil Science). MLS is supported by the Louisiana Board of Regents.

References

[1] R.M. Bailliard-Letournel, A.J.G. Cobo, C. Mirodatos, M. Primet, J.A. Dalmon, Catal. Lett. 2 (1989) 149–156.
[2] A. Kiennemann, C. Diagne, J.P. Hindermann, P. Chaumette, P. Courty, Appl. Catal. 53 (1989) 197–216.
[3] N. Mouaddib, V. Perrichon, G.A. Martin, Appl. Catal. A: Gen. 118 (1994) 63–72.
[4] P. Chaumette, P. Courty, A. Kiennemann, R. Kieffer, S. Boujana, G.A. Martin, J.A. Dalmon, P. Meriaudeau, C. Mirodatos, B. Holhein, D. Mausbeck, A.J. Hubert, A. Germain, A. Noels, Ind. Eng. Chem. Res. 33 (1994) 1460–1467.
[5] J.E. Baker, R. Burch, S.J. Hibble, P.K. Loader, Appl. Catal. 65 (1990) 281–292.
[6] J.A. Dalmon, P. Chaumette, C. Mirodatos, Catal. Today 15 (1992) 101–127.
[7] J.A. Rodriguez, J.Y. Kim, J.C. Hanson, M. Perez, A.I. Frenkel, Catal. Lett. 85 (2003) 247–254.
[8] J.Y. Kim, J.A. Rodriguez, J.C. Hanson, A.I. Frenkel, P.L. Lee, J. Am. Chem. Soc. 125 (2003) 10684–10692.
[9] S.D. Robertson, B.D. McNicol, J.H. Debaas, S.C. Kloet, J.W. Jenkins, J. Catal. 37 (1975) 424–431.
[10] G.C. Bond, S.N. Namijo, J.S. Wakeman, J. Mol. Catal. 64 (1991) 305–319.
[11] C.J.G. van der Grift, A. Mulder, J.W. Geus, Appl. Catal. 60 (1990) 181–192.
[12] A.J. Marchi, J.L.G. Fierro, J. Santamaria, A. Monzon, Appl. Catal. A: Gen. 142 (1996) 375–386.
[13] Z.L. Wang, Q.S. Liu, J.F. Yu, T.H. Wu, G.J. Wang, Appl. Catal. A: Gen. 239 (2003) 87–94.
[14] Y. Matsumura, H. Ishibe, J. Catal. 268 (2009) 282–289.
[15] A.Y. Khodakov, J. Lynch, D. Bazin, B. Rebours, N. Zanier, B. Moisson, P. Chaumette, J. Catal. 168 (1997) 16–25.
[16] E. van Steen, G.S. Sewell, R.A. Makhothe, C. Micklethwaite, H. Manstein, M. deLange, C.T. Oconnor, J. Catal. 162 (1996) 220–229.
[17] A.M. Saib, A. Borgna, J. van de Loosdrecht, P.J. van Berge, J.W. Geus, J.W. Niemantsverdriet, J. Catal. 239 (2006) 326–339.
[18] G. Fierro, M. Lo Jacono, M. Inversi, R. Dragone, P. Porta, Top. Catal. 10 (2000) 39–48.
[19] D.S. Brands, E.K. Poels, A. Bliek, Appl. Catal. A: Gen. 184 (1999) 279–289.
[20] D.V. Cesar, C.A. Perez, V.M.M. Salim, M. Schmal, Appl. Catal. A: Gen. 176 (1999) 205–212.
[21] S.Y. Deng, W. Chu, H.Y. Xu, L.M. Shi, L.H. Huang, J. Nat. Gas Chem. 17 (2008) 369–373.
[22] B. Ravel, M. Newville, J. Synchrotron Radiat. 12 (2005) 537–541.
[23] G.P. Williams, Electron binding energies, in: A.C. Thompson, D. Vaughan (Eds.), X-ray Data Booklet, second ed., Lawrence Berkeley National Laboratory, Berkeley, 2001, pp. 1-1–1-7.
[24] N.D. Subramanian, G. Balaji, C.S.S.R. Kumar, J.J. Spivey, Catal. Today 147 (2009) 100–106.
[25] N. Tien-Thao, H. Alamdari, M.H. Zahedi-Niaki, S. Kaliaguine, Appl. Catal. A: Gen. 311 (2006) 204–212.
[26] E.B. Batyrev, J.C. van den Heuvel, J. Beckers, W.P.A. Jansen, H.L. Castricum, J. Catal. 229 (2005) 136–143.
[27] G. Jacobs, M.C. Ribeiro, W.P. Ma, Y.Y. Ji, S. Khalid, P.T.A. Sumodjo, B.H. Davis, Appl. Catal. A: Gen. 361 (2009) 137–151.
[28] T.T. Nguyen, M.H. Zahedi-Niaki, H. Alamdari, S. Kaliaguine, Int. J. Chem. React. Eng. 5 (2007).
[29] G.G. Volkova, T.M. Yurieva, L.M. Plyasova, M.I. Naumova, V.I. Zaikovskii, J. Mol. Catal. A: Chem. 158 (2000) 389–393.
[30] G. Jacobs, Y.Y. Ji, B.H. Davis, D. Cronauer, A.J. Kropf, C.L. Marshall, Appl. Catal. A: Gen. 333 (2007) 177–191.
[31] G.H. Li, L.Z. Dai, D.S. Lu, S.Y. Peng, J. Solid State Chem. 89 (1990) 167–173.
[32] J.I. Di Cosimo, A.J. Marchi, C.R. Apesteguia, J. Catal. 134 (1992) 594–607.
[33] V. Krishnan, R.K. Selvan, C.O. Augustin, A. Gedanken, H. Bertagnolli, J. Phys. Chem. C 111 (2007) 16724–16733.